Dipolar structures in magnetite ferrofluids studied with small-angle neutron scattering with and without applied magnetic field

M. Klokkenburg,[1,*] B. H. Erné,[1] A. Wiedenmann,[2] A. V. Petukhov,[1] and A. P. Philipse[1]
[1]*Van 't Hoff Laboratory for Physical and Colloid Chemistry, Debye Institute, Utrecht University, Padualaan 8, 3584 CH Utrecht, The Netherlands*
[2]*Hahn-Meitner-Institut Berlin, Department SF3, Glienickerstrasse 100, D-14109 Berlin, Germany*
(Received 17 January 2007; revised manuscript received 15 March 2007; published 24 May 2007)

Field-induced structure formation in a ferrofluid with well-defined magnetite nanoparticles with a permanent magnetic dipole moment was studied with small-angle neutron scattering (SANS) as a function of the magnetic interactions. The interactions were tuned by adjusting the size of the well-defined, single-magnetic-domain magnetite (Fe_3O_4) particles and by applying an external magnetic field. For decreasing particle dipole moments, the data show a progressive distortion of the hexagonal symmetry, resulting from the formation of magnetic sheets. The SANS data show qualitative agreement with recent cryogenic transmission electron microscopy results obtained in 2D [Klokkenburg *et al.*, Phys. Rev. Lett. **97**, 185702 (2006)] on the same ferrofluids.

DOI: 10.1103/PhysRevE.75.051408 PACS number(s): 82.70.Dd, 61.12.Ex, 64.70.Nd, 75.50.Mm

I. INTRODUCTION

Ferrofluids are colloidal dispersions of single-domain magnetic particles, electrostatically or sterically stabilized in water or organic solvents. The structural behavior of ferrofluids is mainly governed by the dipolar interaction potential, of which the depth of the potential well cannot be tuned by a magnetic field. This is because the magnetic dipole moments of the particles in ferrofluids are permanent, in contrast to the particles in electrorheological (ER) and magnetorheological (MR) fluids, with an induced dipole moment that depends on the external field strength [1]. In ferrofluids, the maximal dipolar attraction (for two dipoles in head-to-tail configuration) is $V_{max}=-\mu_0\mu^2/(2\pi k_BTd^3)$, where $\mu_0=4\pi\times10^{-7}$ J A^{-2} m^{-1}, μ is the magnetic dipole moment of one particle, k_B is the Boltzmann constant, T is the absolute temperature, and d is the hard core diameter, including the surfactant shell if it is present. When the dipolar attraction exceeds a few k_BT, the dipolar nanoparticles self-assemble into magnetic equilibrium structures such as dipolar chains, as was recently demonstrated in dilute iron [2] and magnetite (Fe_3O_4) [3] dispersions. In an applied magnetic field, the interaction of the dipoles with the field is $\epsilon=-\mu\mu_0H/(k_BT)$, where H is the magnetic field strength. Although V_{max} is not affected by an applied field, the interaction of the particles with the field causes the dipole moments to (partially) align and, hence, the effective attraction to increase. As a result, elongated clusters can form due to lateral interactions between the dipolar chains, yielding semiordered nanoparticle arrangements [2,4–8].

The basic physics of this type of structural transition in which dipolar chains are attracted in the lateral direction is still being debated, particularly since two rigid finite chains are expected to repel each other if they are not in close proximity [9]. Halsey and Toor proposed a mechanism in which thermal fluctuations can induce long-range attraction between two parallel chains, leading to column formation [10]. The long-range interaction between dipolar chains is predicted to be independent of the applied field strength, and it reaches a maximum when the interchain distance is of the same order as the thermal fluctuations of the nanoparticle positions. Dipolar column formation has also been predicted to involve defect-driven coarsening [11] and finite chain length effects [12].

In the case of particles with an induced dipole moment, simulations in the presence of a magnetic field have shown a variety of solid equilibrium phases, among which the body-centered-tetragonal (BCT) and face-centered-cubic (fcc) phases [13–15], that can coexist with the chain phase. Experimentally, magnetic-field-induced order has indeed been observed in ER fluids [13] and MR fluids [16]. For particles with a permanent magnetic dipole moment, for instance in ferrofluids, field-induced structure formation has received less attention. Moreover, the columnar phase with hexagonal symmetry that was predicted by simulations for dipolar spheres confined to two dimensions [17,18] has only recently been observed in real-space experiments [8]. Interestingly, recent SANS experiments on cobalt ferrofluids (3D) in a magnetic field also show the formation of magnetic sheets with hexagonal symmetry [5], though the structure formation and phase behavior of colloidal systems in reduced dimensions is not necessarily equivalent to that of 3D systems [19–21].

Here, we provide a detailed study of well-defined magnetic dipolar colloids as a function of particle size using SANS, both in zero field and in an applied external magnetic field. SANS or SANS with polarized neutrons (SANSPOL) has proven to be a powerful technique to study ferrofluids *in situ*, due to the specific interaction of the neutrons with the magnetic core [22]. The primary goal is to compare zero-field and field-induced dipolar structure formation as observed with SANS with data recently obtained in real space [8]. In particular, we recently analyzed the structure of field-induced bands in real space (2D) in terms of radial distribu-

*Corresponding author. Email address: m.klokkenburg@chem.uu.nl

TABLE I. Sample characteristics of systems $A-C$.

Code	A	B	C
d_{TEM} (nm)	9.6±1.2	16.1±2.6	21.0±2.4
d_{XRD} (nm)	8.7±1.3	15.6±2.5	20.6±3.5
$d_{magnetic}$ (nm)	9.0	13.8	18.4
$\langle d_{SANS} \rangle$ (nm)	9.7±1.9	13.4±2.7	18.1±3.6
μ (10^{-19} A m^2)	1.7	6.6	15.5
dipole-dipole attraction V_{max} (units of k_BT)	0.6	4	9
Interaction (ϵ) with 1 T at 300 K (units of k_BT)	42	162	380
Vol. fract. ϕ (%) (excluding surfactant layer)	0.13	1.41	0.38

tion functions and structure factors [8], and now we compare those results to structure factors obtained from SANS (3D). Both techniques show—among other things—thin bands with a progressive distortion of the local hexagonal symmetry for decreasing particle dipole moments.

This paper is organized as follows. In Sec. II, the technique and the single-particle properties of three colloidal dispersions (A, B, and C) each with a different mean particle size are presented. Section III describes the data analysis of the SANS data. Section IV contains the results that were obtained in reciprocal space under different experimental conditions. The results are discussed in Sec. V and conclusions are drawn in Sec. VI.

II. EXPERIMENTAL

Colloidal dispersions of single-domain magnetite (Fe_3O_4) nanoparticles (encoded A, B, and C) dispersed in decalin ($C_{10}H_{18}$) were prepared according to a method described previously [3]. The particles are coated with two short-chain hydrocarbons, oleic acid and oleylamine, to prevent them from irreversible aggregation. The dispersions were prepared with a small excess of surfactant (1 mM) to prevent surfactant desorption [23]. Steric stabilization of these particles in nonpolar solvents substantially screens van der Waals attractions and introduces steep steric repulsion between the particles at contact. Therefore, the only additional contribution to the pair interaction is a dipolar potential x/r^3, where x is the amplitude depending on the angular orientation of two dipoles at a center-to-center distance r. The strength of the attractions and, consequently, the equilibrium chain length can be tuned by adjusting the volume of the particles and with that the dipole moment [24]. The characteristics of the individual particles are listed in Table I, including the values for the dipolar contact attraction V_{max} between the particles, the interaction of the particles with a magnetic field, and the volume fractions ϕ.

SANS measurements were performed on samples with hydrogenated decalin to study the magnetic structures and on diluted samples consisting of a mixture of H-decalin and D-decalin (deuterated) to probe the core-shell structure of the individual particles. The average particle sizes obtained from fitting SANS data of diluted samples are given in Table I. SANS(POL) measurements were conducted between 100 and 300 K on the V4 [25,26] instrument installed at the BERII reactor of HMI situated in Berlin. The scattering patterns were collected at sample-detector distances of 2, 4, and 12 m, using symmetrical collimations. Scattering patterns that are presented in this paper were collected at a sample-detector distance of 4 m. The wavelength of the neutron beam was $\lambda=0.6$ nm with a wavelength spread of $\delta\lambda/\lambda=0.1$. All data have been corrected pixel by pixel for background, transmission, and detector efficiency, and converted to an absolute scale by referring to the incoherent scattering of a water standard. The scattering length density of the deuterated decalin was $\eta_{solvent}=5.8\times10^{10}$ cm^{-2}, corresponding to 90% of hydrogen exchange by deuterium. For the nuclear and magnetic scattering length densities we used the theoretical values of bulk magnetite $\eta_{nuc}=6.96\times10^{10}$ cm^{-2} and $\eta_{mag}=1.39\times10^{10}$ cm^{-2}, respectively [see Fig. 1(a)]. The horizontal magnetic field (1 T) was aligned perpendicular with respect to the incoming neutron beam. The sample thickness was 1 mm.

III. DATA ANALYSIS

SANS and SANSPOL

For polarized neutrons (SANSPOL) the scattering intensity depends on the polarization state of the neutrons, which can be parallel ($-$) or antiparallel ($+$) to the applied magnetic field. When the magnetic dipole moments are fully aligned along an external field **H** the two intensities are given by

$$I(-,+)(Q) = N_P \int_j N_j(R)[F_N^2(Q) + \sin^2\alpha(F_M^2(Q)) \pm 2F_N(Q)F_M(Q)]S(Q,\alpha)dR, \quad (1)$$

where $N_j(R)$ is the size distribution of particles with number density N_P. $F_N(Q)$ and $F_M(Q)$ are the nuclear and magnetic form factors of the particles, respectively. α is the angle between the scattering vector **Q** and the magnetic field direction. $S(Q,\alpha)$ is an anisotropic structure factor that accounts for the local order of the particles and which for diluted systems is $S(Q)=1$. $S(Q)$ is related to the pair distribution function $g(r)$ by the Fourier transform $S(Q)=1+N_P\int[g(r)-1]\exp(iQr)dr$. Along the magnetic field the intensity is independent of the polarization state and results

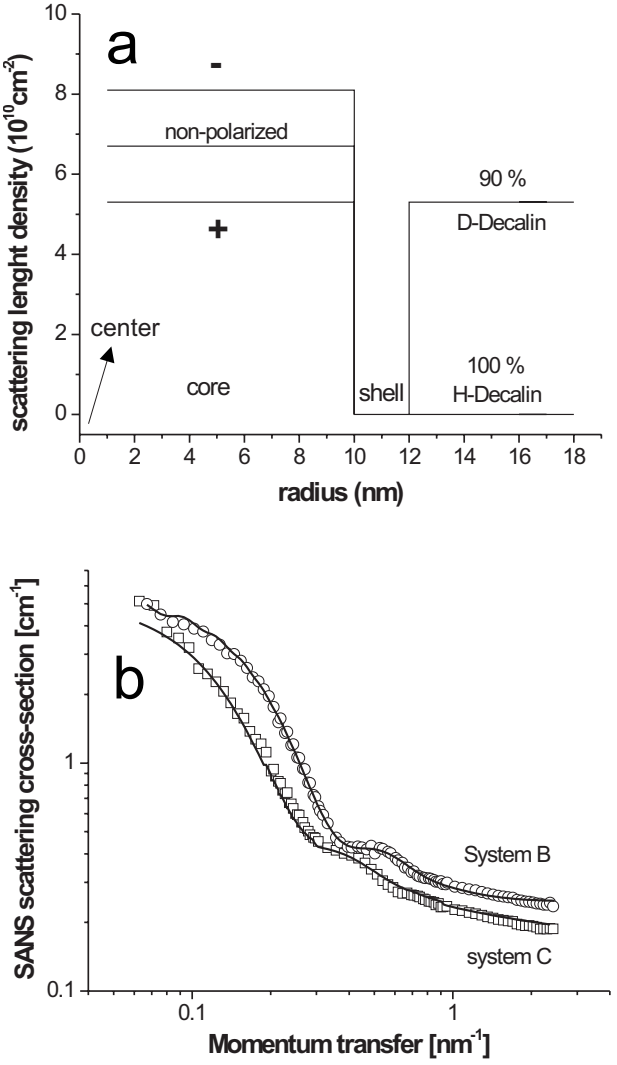

FIG. 1. (a) Schematic representation of the SANS fit model with the particle radius of system *C*. The *x* axis corresponds to the distance from the center of the particle. For the (−) curve the magnetic and nuclear scattering length densities were added, whereas for the (+) curve the magnetic scattering length density was subtracted from the nuclear scattering length density. (b) Zero-field scattering data for dilute samples of system *B* (○) and system *C* (□) (radial average), the solid line showing a fit using the core-shell model [Eq. (2)].

from nuclear contrast only, while for **Q** perpendicular to **H** the polarization dependent magnetic contribution is maximum. In the core-shell model assumed here, the particles contain a magnetic core of radius *R* and a nonmagnetic shell of thickness *D*, the form factors are given by

$$F_{c\text{-}sh}(Q) = [(\Delta\eta_1 - \Delta\eta_2) f_{sph}(QR) + \Delta\eta_2 f_{sph}(Q(R+D))]V_p, \tag{2}$$

where $f_{sph}(x)$ is the well-known shape factor for spheres: $f_{sph}(x) = 3[\sin(x) - x\cos(x)]/x^3$, where x equals QR. The scattering contrasts for nuclear scattering are given by $\Delta\eta_1^{nuc} = \eta_c^{nuc} - \eta_{solvent}$ and $\Delta\eta_2^{nuc} = \eta_{sh}^{nuc} - \eta_{solvent}$ while for the magnetic scattering $\Delta\eta_1^{mag} = \eta_{\mathbf{M}} = 0.27 \times 10^{-12} \Sigma c_i \mathbf{M_i}^{\perp}/\Omega_i$, where c_i and Ω_i are the concentrations and atomic volumes of the elements, and where only the projection of the magnetic moment $\mathbf{M_i}^{\perp}$ onto a plane perpendicular to the scattering vector **Q** contributes to the interaction. $\mathbf{M_i}^{\perp}$ is given in units of Bohr magnetons μ_B. For the nonmagnetic shell $\Delta\eta_2^{mag} = 0$. The intensity difference between the two polarization states indicates a nuclear-magnetic cross term

$$I^-(Q,\alpha) - I^+(Q,\alpha) = 4F_N F_M S(Q,\alpha)\sin^2\alpha. \tag{3}$$

The average $(I^+ + I^-)/2$ of both polarization states corresponds to the scattering of nonpolarized neutrons, given by

$$[I^+(Q) + I^-(Q)]/2 = N_P \int_j N_j(R)[F_N^2(Q) + F_M^2(Q)\sin^2\alpha]S(Q)dR. \tag{4}$$

In zero magnetic field the magnetic moments of the superparamagnetic particles are distributed randomly and the scattering is isotropic and given by

$$I(Q)_{H=0} = N_P \int_j N_j(R)[F_N^2(Q) + 2/3F_M^2(Q)]S(Q)dR. \tag{5}$$

In the case of weak magnetic fields the intensities are determined by Langevin statistics [27,28].

IV. RESULTS

A. Room temperature measurements

To characterize the colloidal particles, a core-shell model was used [Eq. (2)] to fit the scattering curves of diluted samples, which are expected to contain no structures (dilution with a factor of 10 compared to the original dispersions listed in Table I). The scattering intensities for the diluted systems were fitted according to Eq. (1) using $S(Q)=1$ and the theoretical contrast values. Figure 1(a) shows a schematic representation of the different scattering length densities of the core, the shell, and the solvents. The size of the core and the thickness of the shell were determined from a fit of the scattering curves of dilute samples [Fig. 1(b)]. In all cases, volume weighted average core diameters $\langle d_{core}\rangle$ ranging from 9.7 to 18.1 nm were obtained that agree well with the average particle sizes from TEM, x-ray diffraction (XRD), and magnetization curves (Table I). From fitting the SANS data, a surfactant shell thickness of 2.1 nm was obtained, which is in line with $g(r)$ data obtained from analyzing cryogenic transmission electron microscopy (cryo-TEM) images that indicate a particle separation in a chain of one times the diameter d plus 3–4 nm [24]. Since the thickness of the surfactant layer agrees with the length of one oleic acid or oleylamine molecule, this indicates that the particles are grafted with a monolayer of surfactants.

Figure 2 gives the 2D SANS scattering patterns of systems *A*–*C* in zero field and in 1 T. As can be inferred from the zero-field data, the patterns are isotropic as long as the dipole-dipole attractions do not exceed $2k_BT$. For system *C* at 0 T, the SANS scattering pattern is slightly anisotropic, showing more intensity in the vertical direction and suggest-

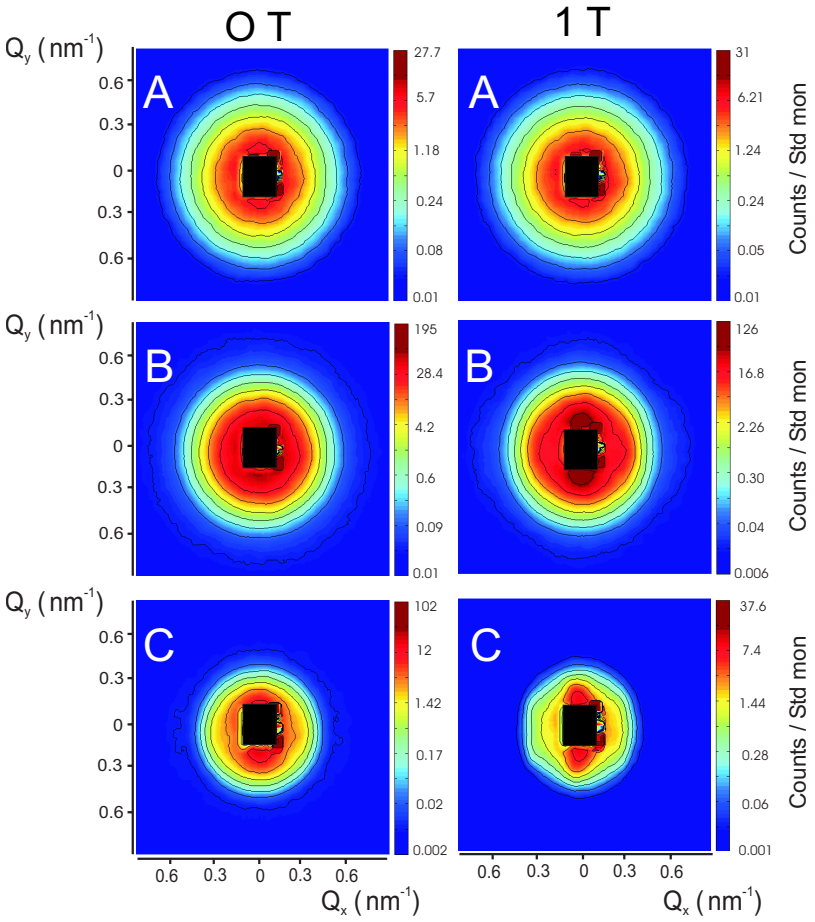

FIG. 2. (Color online) 2D SANS patterns of systems $A-C$ at 300 K in zero field (left panels) and at 1 tesla (right panels). The horizontal magnetic field was aligned perpendicular to the incoming neutron beam. The spectra are normalized to standard monitor (std. mon.).

ing the presence of aligned magnetic structures. This alignment is due to the presence of a small remanent magnetic field of the electromagnet of the order of 5 mT, which leads to an interaction of a few k_BT between single dipoles and the field. The scattering intensity scales with Q^{-1} at low Q values, which is typical for linear objects [5,29] and therefore supports the presence of dipolar chains, as observed recently in thin vitrified films of ferrofluids [Fig. 3(a)] [8]. This scaling behavior was only observed in system C.

To see whether magnetic structures can be induced in dispersions with smaller particles (systems A and B), we applied a horizontal magnetic field of 1 T, which causes alignment of the magnetic moments and with that facilitates a stronger mean attraction. As Fig. 2 shows, the scattering patterns are all anisotropic in an applied field of 1 T, even for system A, which contains particles with relatively weak dipoles. They nevertheless have $42k_BT$ of interaction with the field (Table I). Hexagonal symmetry emerges in system C, where ϵ is more than 150 (Table I), suggesting that the strings that are already present in zero field [see Fig. 3(a)] assemble into larger structures.

B. Low temperature measurements

To amplify the effects of dipolar attractions, we lowered the temperature to 100 K, far below the melting point of the pure solvent (242 K) and below the melting trajectory of the dispersion [30]. Consequently, the dipolar structures become

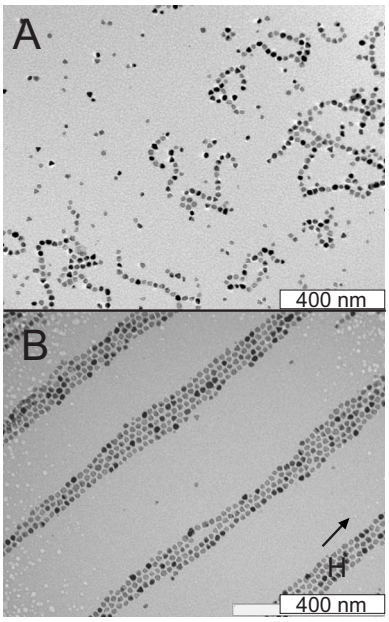

FIG. 3. (a) Typical *in situ* cryo-TEM images of vitrified films of magnetite dispersion C in zero field ([24]). (b) In a homogeneous magnetic field (0.2 T), a transition occurs to equal-spaced columns that exhibit hexagonal symmetry [8].

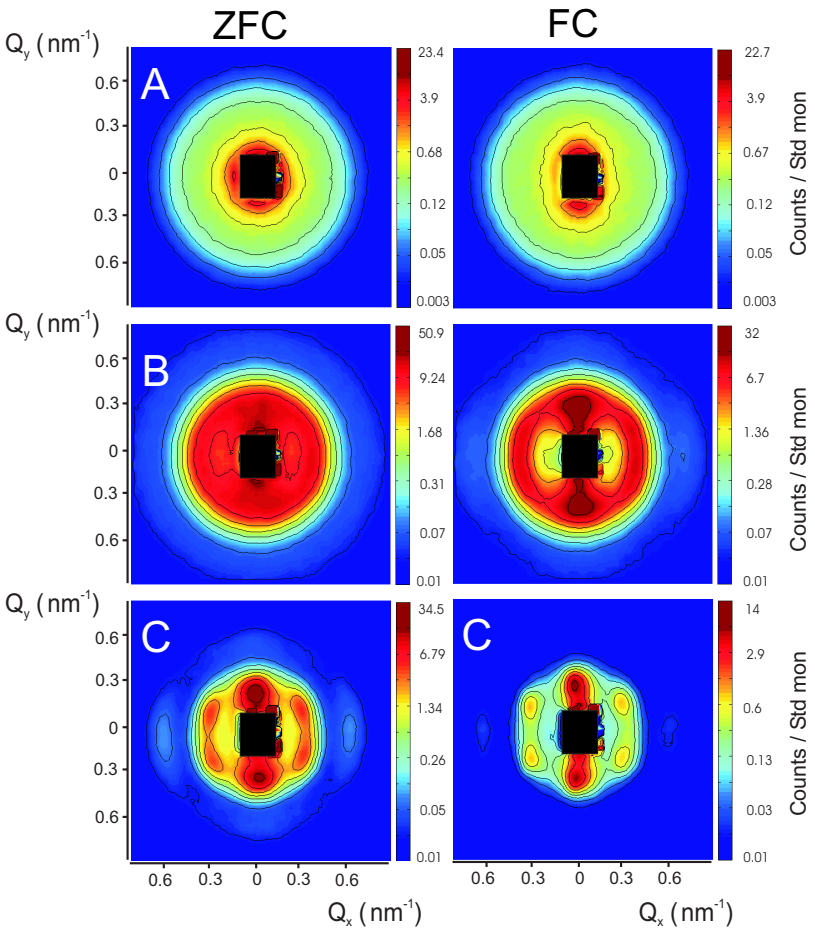

FIG. 4. (Color online) 2D SANS scattering patterns of systems $A-C$ cooled in zero field (left panels) and 1 T (right panels) all recorded at 100 K. The spectra are normalized to standard monitor (std. mon.).

fixed in a solid matrix and the magnetic dipoles of the individual particles become blocked at their blocking temperature T_{block}.

Figure 4 indicates that on reducing the temperature to 100 K, the SANS scattering patterns are profoundly affected (compare to Fig. 2). The hexagonal symmetry of the magnetic structures becomes more pronounced. Note the gradual transition from an almost isotropic pattern in the case of small magnetic particles (upper left panel in Fig. 4), where the dipole-dipole attractions are less than $1k_BT$, to a hexagonal scattering pattern when relatively large dipoles are involved that are aligned and strongly interact (lower right panel in Fig. 4). This is a new illustration that the many-particle structures depend on both the magnetic field strength and the dipole moments of the particles. Particularly in system C, it is interesting to see the clear structural differences between the field-cooled and zero-field-cooled situations; cooling in field results in a distinct hexagon with two additional well-defined peaks in the direction of the field (horizontal), whereas cooling "without field" (a remanent field of 5 mT is present) leads to a less sharply defined scattering pattern. In the field-cooled scattering pattern of system C in Fig. 4, four maxima can be observed at constant scattering vectors of $Q_1=0.36$ nm^{-1} and at angles of ±30° with respect to the horizontal direction of the magnetic field. Furthermore, two peaks are present, at $Q_2=0.34$ nm^{-1} in the 90° direction and at $Q_3=0.61$ nm^{-1} in the horizontal (0°) direction. The peaks can be assigned to different reflections as is schematically depicted in Fig. 5.

To elucidate the hexagonal symmetry of the field-cooled magnetic structures in system C, we first calculated the radial average of a thin shell sector with an average radius of 0.36 nm^{-1}, which comprises the six distinguishable peaks Q_1 and Q_2. Figure 6 reflects the scattering intensity as a function of the azimuthal angle at temperatures between 300 and

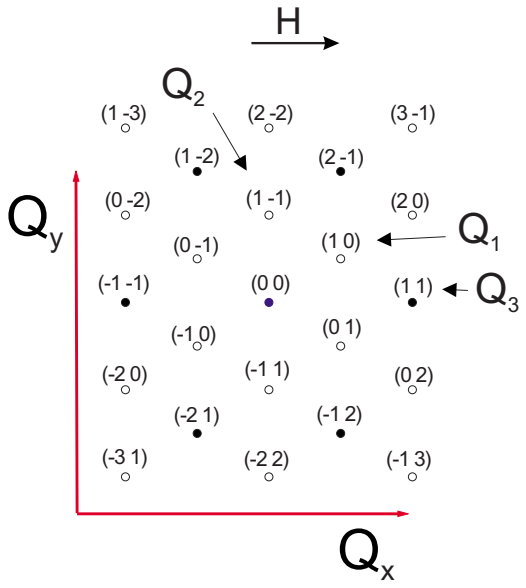

FIG. 5. (Color online) The positions of the Q_1, Q_2, and Q_3 peaks in the hexagonal reciprocal lattice are indicated with arrows.

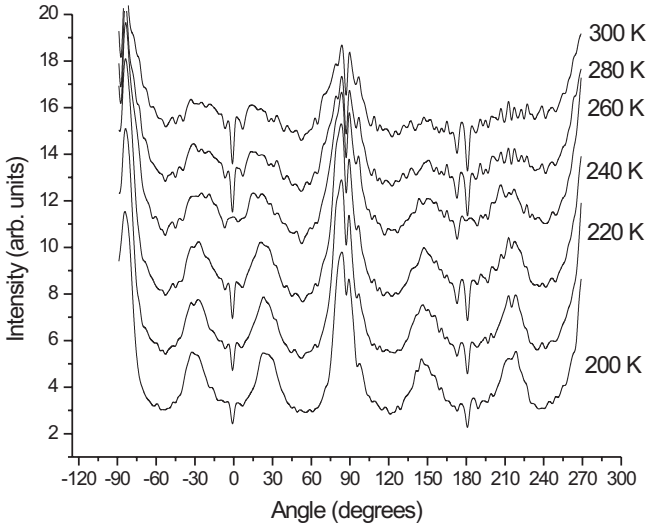

FIG. 6. SANS intensity of system *C* after field cooling (1 T) integrated over 0.25 $nm^{-1} < Q < 0.47$ nm^{-1} as a function of the azimuthal angle between the horizontal field and *Q*. The curves are shifted vertically for clarity to show the gradual transition to the hexagonal structure on reducing the temperature.

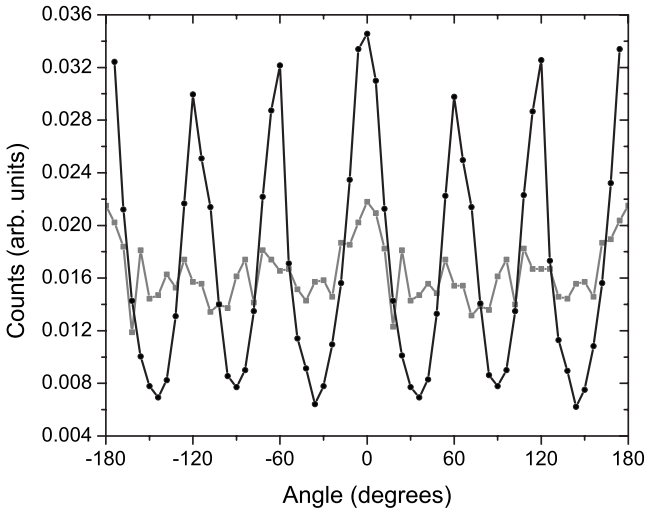

FIG. 7. Nearest neighbor angle distributions for the *B* particles (gray) and the *C* particles (black), as obtained from cryo-TEM images [8]. The magnetic field is along the zero degree direction.

200 K. The graphs corroborate the presence of a hexagonal structure, as the peak positions are separated by about 60°, and they show that the structure gradually sets in as the temperature is reduced from room temperature to 240 K. The peak positions and the shape of the peaks are neither profoundly influenced when the temperature is reduced, nor when the field strength is varied.

The hexagonal symmetry can be explained by magnetic sheets that form in a homogeneous magnetic field, as is shown in Fig. 3(b) [8]. The nearest neighbor angle distributions for the particles in the *B* and *C* system, as obtained from the cryo-TEM images, also show that the orientational order is enhanced with increasing dipolar interactions (see Fig. 7). Moreover, the orientational order as depicted in Fig. 7 for system *C* qualitatively agrees with the angle distributions in Fig. 6. The calculated structure factor profiles from the cryo-TEM images are depicted in Fig. 8, including the corresponding sector averages for $\alpha=30°$ and 90° which show peaks at $Q=0.28$ nm^{-1} and $Q=0.31$ nm^{-1}.

To be able to distinguish the nuclear from the magnetic scattering contribution, we performed SANSPOL measurements on system *C*. Figure 9 demonstrates the different scattering patterns obtained with two different polarization states I^+ and I^-. Both states show hexagonal symmetry and the Q_3 peaks at 0.61 nm^{-1} which are due to fully nuclear scattering contributions. The intensity difference between $I^+ - I^-$ that comprises the nuclear-magnetic cross term is confined to the vertical axis suggesting a magnetic structure that is aligned in the horizontal direction in real space.

Figure 10 displays the SANSPOL intensities I^+ and I^- obtained for system *C* averaged over four azimuth sectors of 15° in width. In the 0° sector, where the intensity is fully due to the nuclear contrast, a peak at Q_3 as well as a peak at $Q=0.34$ nm^{-1} can be clearly distinguished. The maximum at $Q=0.34$ nm^{-1} reflects diffuse residual intensity present along the vertical direction between the two Q_1 peaks, which can be ascribed to the first order diffraction peak of single chains. In the sector $\alpha=30°$, where only a slight difference in the SANSPOL intensities is observed, a well-defined peak is present at Q_1. In contrast, in the $\alpha=60°$ sector only a broad shoulder exists, though the two SANSPOL intensities now slightly differ. Besides the fact that the intensities are more strongly dependent on the polarization state in the vertical direction ($\alpha=90°$), the peak is broadened and shifted to $Q=0.34$ nm^{-1}. This means that the average interparticle distance is 10% larger in the direction perpendicular to the magnetic field than in the direction parallel to the magnetic field,

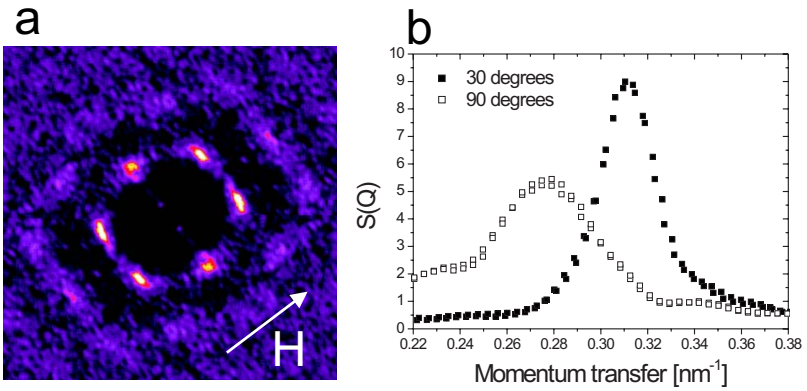

FIG. 8. (Color online) (a) Scattering pattern obtained from the cryo-TEM images prepared in field [8] [see Fig. 3(b)] and (b) the corresponding sector averages (30° and 90°). In (a), the brighter the peaks are, the stronger the intensity is.

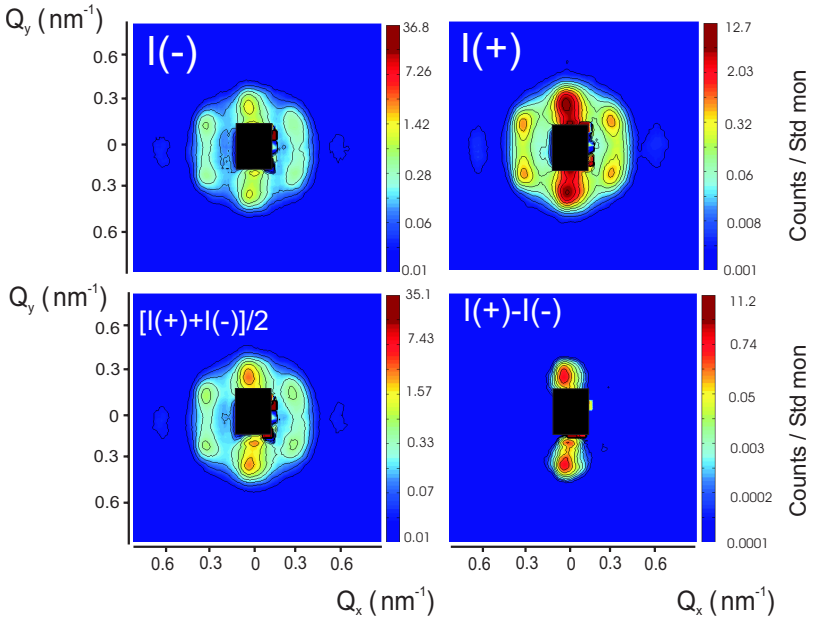

FIG. 9. (Color online) 2D SANSPOL intensities for system *C* in a horizontal magnetic field of 1 T at 100 K. I^+ refers to the neutron spin antiparallel to the field H and I^- to the neutron spin parallel to H. The average $[I^+ + I^-]/2$ corresponds to the nonpolarized scattering pattern [Fig. 4(c), field-cooled], and $I^+ - I^-$ reflects only the nuclear-magnetic cross term resulting from magnetic particles only [Eq. (1)]. The spectra are normalized to standard monitor (std. mon.).

which is in line with cryo-TEM results that show a similar difference in spacing in the lateral and longitudinal direction [see Fig. 8(b)]. The structure factors $S(Q,\alpha)$ for the four orientations, shown in Fig. 11, were obtained by dividing the measured intensities $I^{\pm}$ by those obtained from a fit to scattering data of diluted samples; again the peak positions at $Q_1=0.36$ nm^{-1} for $\alpha=30°$, $Q_2=0.34$ nm^{-1} for $\alpha=90°$, and $Q_3=0.61$ nm^{-1} for $\alpha=0°$ indicate the distortion in the lateral direction. Note the qualitative similarities between these structure factors and the structure factors obtained from the cryo-TEM images [Fig. 8(b)]; they both indicate a distorted symmetry.

Comparing the peak positions of Q_1 and Q_3 yields a ratio of 1.65, close to the expected value $\sqrt{3}$ for hexagonal symmetry. The hexagonal lattice constant can be calculated using $Q(hk)=2\pi\sqrt{4(h^2+k^2+hk)/3a^2}$, yielding $a_{hex}=19.6$ nm based on Q_1 (100) and $a_{hex}=20.6$ nm based on Q_3 (110), suggesting that the structures are slightly distorted. Assuming that line broadening is dominated by the size of the crystals, the full width at half maximum (FWHM) of both reflections gives a correlation length of approximately 60 nm, which roughly corresponds to three particle diameters. This qualitatively agrees with the cryo-TEM image in Fig. 3(b) that shows similar correlation lengths, confirming predominantly local order. Similar lattice constants have been obtained on concentrated Co ferrofluids dispersed in toluene and in technical oil [5,31].

The obtained SANS scattering patterns were compared to simulated diffraction data for body-centered tetragonal (BCT), face-centered cubic (fcc), and random-stacking hexagonal close-packed (RHCP) structures (see Fig. 12), which have been observed in simulations for spherical colloids carrying a dipole moment [15]. In all cases, one of the crystallographic directions was assumed to be fixed by the external magnetic field while orientational averaging was done for the other two directions. Interestingly, the simulation results for all three structures (see Fig. 12) were found to be not in line with the experimental data. Clearly, additional peaks should appear if it concerns a three-dimensional stacking of the particles. However, the observed broadening of the Q_2 peak to low Q values might nevertheless be an indication for interplane correlations, though the Q range would correspond to a much larger (approximately 15%) interplanar distance than the one expected in a close-packed structure. Our results thus suggest that at these volume fractions formation of (quasi-)2D bands with weak positional interband correlations between the bands also occurs in 3D suspensions.

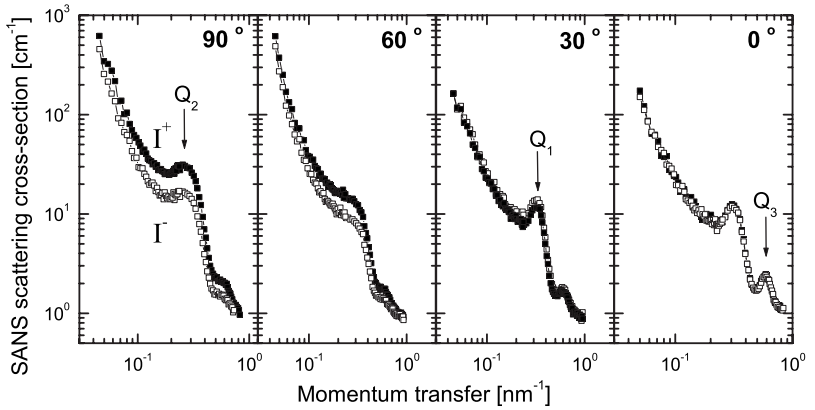

FIG. 10. SANSPOL intensities I^+ (black squares) and I^- (open squares) of system *C* (100 K) averaged over azimuth sectors of 15° in width, with sector centers at 90° (⊥), 60°, 30°, 0° (∥). The magnetic field was applied perpendicular to the incident neutron beam.

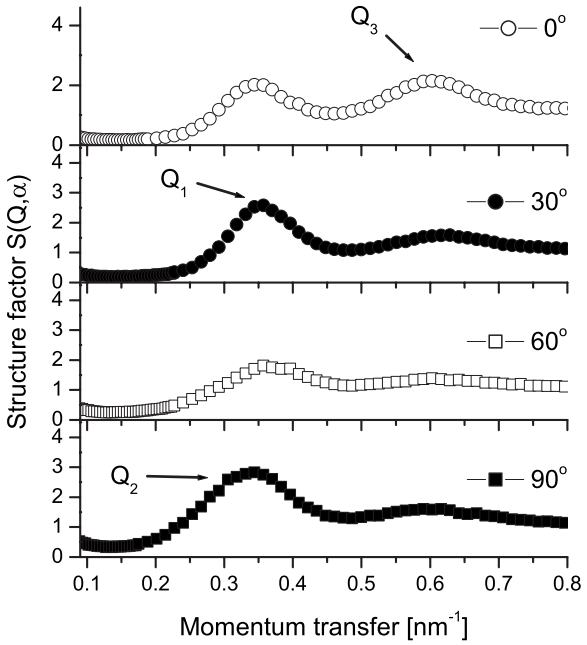

FIG. 11. Obtained structure factors $S(Q,\alpha)$ for system C (100 K) for sectors $\alpha=0°$, $30°$, $60°$, $90°$.

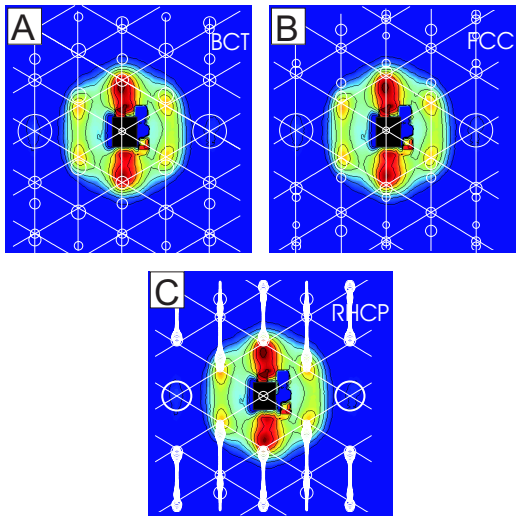

FIG. 12. (Color online) Simulated diffraction patterns (white open circles) for BCT (a), fcc (b), and RHCP (c) crystal structures. The simulated patterns are scaled to the 110 reflection and are placed on top of the original scattering patterns that were obtained at 100 K and 1 T. The size of the symbols is proportional to the square root of the integrated intensity. For clarity, the hexagonal symmetry of the pattern is underlined (white lines).

V. DISCUSSION

Magnetic field-induced structures in colloidal dispersions of magnetic dipolar colloids were studied as a function of particle size using SANS. The important observation is a clear gradual transition from isotropic particle configurations for weak dipolar interactions (system A) to bands with hexagonal symmetry for strong dipolar fluids (system C).

In system C, due to the strong dipole-dipole interaction, which is enhanced by the alignment of the dipoles in an external magnetic field, sheets are formed that exhibit hexagonal symmetry, manifesting the structures observed with cryo-TEM in the presence of a homogeneous magnetic field [Fig. 3(b), [8]]. Within these bands, two neighboring chains are generally displaced by half a hard-sphere diameter, which is energetically favorable since this leads to short range attraction [9,10,13,32]. For rigid aligned chains that are out of registry, the lateral chain-chain interaction scales with the dipole-dipole attraction and with the length of the chains [9].

In system B, where the dipole-dipole attraction is only $4k_BT$, the relatively short zero-field dipolar chains (that have been previously observed in this system [3]) become correlated in the presence of a homogeneous magnetic field. The interaction of the particles with the field is strong enough ($>160k_BT$) to align the dipolar chains and the individual magnetic moments. Consequently, the alignment causes attractive forces in the lateral direction between existing magnetic chains. However, since these attractions are expected to be relatively low, this results in the formation of diffuse bands without local orientational order, in line with recent cryo-TEM observations [8]. Therefore, the observed scattering patterns display no clear hexagonal symmetry.

Thermal fluctuations [32], defective chains [11], or chain bending in general [12] can induce variations in the dipole moment density and, consequently, long-range coupling between one-dimensional structures in colloidal dispersions. The distorted hexagonal symmetry that is observed for system C with both SANS and cryo-TEM suggests that defects or thermal fluctuations may also play such a role here.

VI. CONCLUSION

The studied colloidal magnetic particles can be well described by the applied core-shell model, resulting in a core-shell structure that agrees with the structure obtained from real-space data. We have demonstrated that colloidal dispersions of sterically stabilized nanoparticles with a sufficiently large permanent magnetic dipole moment form bands with distorted hexagonal symmetry in the presence of an in-plane magnetic field. The scattering data qualitatively agree with cryo-TEM data obtained in 2D for the same systems. The obtained scattering patterns are not in line with common colloidal crystal structures and therefore suggest that the formation of (quasi-)2D bands with weak correlations between the bands also occurs in 3D suspensions.

ACKNOWLEDGMENTS

We thank Bonny Kuipers for his help with the temperature-dependent susceptibility measurements. We also express our thanks to Roel Dullens for fruitful discussions. This research has been supported by the European Commission under the 6th Framework through the Key Action: Strengthening the European Research Infrastructures, Contract No. RII-CT-2003-505925.

[1] A. Yethiraj and A. van Blaaderen, Nature (London) **421**, 513 (2003).
[2] K. Butter, P. H. H. Bomans, P. M. Frederik, G. J. Vroege, and A. P. Philipse, Nat. Mater. **2**, 88 (2003).
[3] M. Klokkenburg, C. Vonk, E. M. Claesson, J. D. Meeldijk, B. H. Erné, and A. P. Philipse, J. Am. Chem. Soc. **126**, 16706 (2004).
[4] L. N. Donselaar, P. M. Frederik, P. Bomans, P. A. Buining, B. M. Humbel, and A. P. Philipse, J. Magn. Magn. Mater. **201**, 58 (1999).
[5] A. Wiedenmann, A. Hoell, M. Kammel, and P. Boesecke, Phys. Rev. E **68**, 031203 (2003).
[6] Y. Lalatonne, J. Richardi, and M. P. Pileni, Nat. Mater. **2**, 121 (2004).
[7] G. J. Cheng, D. Romero, G. T. Fraser, and A. R. H. Walker, Langmuir **26**, 12055 (2005).
[8] M. Klokkenburg, B. H. Erné, J. D. Meeldijk, A. Wiedenmann, A. V. Petukhov, R. P. A. Dullens, and A. P. Philipse, Phys. Rev. Lett. **97**, 185702 (2006).
[9] E. M. Furst and A. P. Gast, Phys. Rev. E **62**, 6916 (2000).
[10] T. C. Halsey and W. Toor, J. Stat. Phys. **61**, 1257 (1990).
[11] J. E. Martin, K. M. Hill, and C. P. Tigges, Phys. Rev. E **59**, 5676 (1999).
[12] M. Gross and S. Kiskamp, Phys. Rev. Lett. **79**, 2566 (1997).
[13] R. Tao and J. M. Sun, Phys. Rev. Lett. **67**, 398 (1991).
[14] B. Groh and S. Dietrich, Phys. Rev. E **63**, 021203 (2001).
[15] A. P. Hynninen and M. Dijkstra, Phys. Rev. E **72**, 051402 (2005).
[16] M. Ivey, J. Liu, Y. Zhu, and S. Cutillas, Phys. Rev. E **63**, 011403 (2001).
[17] A. Satoh, R. W. Chantrell, S. I. Kamiyama, and G. N. Coverdale, J. Colloid Interface Sci. **178**, 620 (1996).
[18] J. J. Weis, Mol. Phys. **103**, 7 (2005).
[19] S. Neser, C. Bechinger, P. Leiderer, and T. Palberg, Phys. Rev. Lett. **79**, 2348 (1997).
[20] F. Ramiro-Manzano, F. Meseguer, E. Bonet, and I. Rodriguez, Phys. Rev. Lett. **97**, 028304 (2006).
[21] D. R. Nelson, *Defects and Geometry in Condensed Matter Physics* (Cambridge University Press, Cambridge, 2002), pp. 68–91.
[22] J. B. Hayter, J. Appl. Crystallogr. **21**, 737 (1988).
[23] M. Klokkenburg, J. Hilhorst, and B. H. Erné, Vib. Spectrosc. **43**, 243 (2007).
[24] M. Klokkenburg, R. P. A. Dullens, W. K. Kegel, B. H. Erné, and A. P. Philipse, Phys. Rev. Lett. **96**, 037203 (2006).
[25] A. Wiedenmann, Mater. Sci. Forum **312-314**, 315 (1999).
[26] T. Keller, T. Krist, A. Danzig, U. Keiderling, F. Mezei, and A. Wiedenmann, Nucl. Instrum. Methods Phys. Res. A **451**, 474 (2000).
[27] A. Wiedenmann, Physica B **297**, 226 (2001).
[28] A. Wiedenmann, in *Small Angle Neutron Scattering Investigations of Magnetic Nanostructures, Neutron Scattering from Magnetic Materials*, edited by T. Chatterji (Elsevier, Amsterdam, 2006) pp. 473–520.
[29] O. Glatter and O. Kratky, *Small Angle X-Ray Scattering* (Academic Press, London, 1982).
[30] M. Klokkenburg, B. H. Erné, and A. P. Philipse, Langmuir **21**, 1187 (2005).
[31] A. Wiedenmann and A. Heinemann, J. Magn. Magn. Mater. **289**, 58 (2005).
[32] T. C. Halsey and W. Toor, Phys. Rev. Lett. **65**, 2820 (1990).